Resonance of geometric quantities and hidden symmetry in the asymmetric Rabi model

Qinjing Yu [1] and Zhiguo Lü [1,2,*]

[1]*Key Laboratory of Artificial Structures and Quantum Control (Ministry of Education), School of Physics and Astronomy, Shanghai Jiao Tong University, Shanghai 200240, China*
[2]*Collaborative Innovation Center of Advanced Microstructures, Nanjing University, Nanjing 210093, China*

We present the interesting resonance of two kinds of geometric quantities, namely, the Aharonov-Anandan phase and the time-energy uncertainty, and reveal the relation between resonance and the hidden symmetry in the asymmetric Rabi model by numerical and analytical methods. By combining the counter-rotating hybridized rotating-wave method with time-dependent perturbation theory, we solve systematically the time evolution operator and then obtain the geometric phase of the Rabi model. In comparison with the numerically exact solutions, we find that the analytical results accurately describe the geometric quantities in a wide parameter space. We unveil the effect of the bias on the resonance of geometric quantities: (1) the positions of all harmonic resonances stemming from the shift of the Rabi frequency at the presence of the bias, and (2) the occurrence of even order harmonic resonance due to the bias. When the driving frequency is equal to the subharmonics of the bias, the odd higher-order harmonic resonances disappear. Finally, the hidden symmetry has a resemblance to that of the quantum Rabi model with bias, which indicates the quasienergy spectra are similar to the energy spectra of the latter.

I. INTRODUCTION

Since the geometric phase of Berry's seminal work was introduced in the cyclic evolution of a system under adiabatic condition [1], its effects have been discovered and experimentally measured in various fields of physics [2–11] as well as chemistry [12]. The geometric property of Berry's phase visually lies in that it merely depends on the solid angle subtended by the closed path that the parameters traverse. Aharonov and Anandan (AA) extended Berry's phase to nonadiabatic cases [13,14], removing the adiabatic restriction and only assuming that the initial and final states of the quantum system differ by a total phase factor. Besides theoretical significance, the AA phase has important applications to nonadiabatic geometric gates in quantum computation, with internal resiliency to certain noises and control errors [15–17]. Furthermore, Samuel and Bhandari developed the geometric phase in a general setting without the assumption of cyclic evolution [18]. All these phases are determined by the curve $\mathcal{C}$ that the quantum state traverses in the projective Hilbert space $\mathcal{P}$ and are thus defined as geometric quantities [19].

Time-energy uncertainty, as one of the most fundamental quantities in quantum mechanics, is also proved to be a geometric quantity [19,20]. Although the proposal of the uncertainty principle for time and energy even dates back to the origin of quantum mechanics in the 1920s, it is understood as setting a fundamental limit on the rate of quantum dynamics in its modern formulation [21–24] and is thus widely employed in studies on the speed of gate operations in quantum com-

putation [25–28], the precision of measurement in quantum metrology [29–32], and so on. With the rapid development of technologies in manipulating quantum systems, it has received increasing attention as the basis for optimal control theory [33–36].

The semiclassical Rabi model [37,38], which describes a two-level system coupled with a classical monochromatic periodic field, is a typical quantum model exhibiting the properties of geometric quantities. Its studies have a rich history for both experimental and theoretical investigations [39–47], and nowadays this model is widely applied in quantum information technology [48–50]. It is found that there are a wide variety of interesting dynamical features in this model, such as well-known Rabi oscillations, Bloch-Siegert shifts, coherent destruction of tunneling (CDT) [51], driving-induced tunneling oscillations (DITO) [52], and plateau dynamics [53]. In this work we consider the asymmetric semiclassical Rabi model, where a bias term is taken into account. The bias breaks the symmetry of the semiclassical Rabi model [54], which contributes to the complexity and phenomena different from those of the symmetric Rabi model. This allows for the representation of energy biases between the two states of a flux qubit [55].

While previous studies have primarily concentrated on the dynamics of the asymmetric semiclassical Rabi model [56,57], including phenomena such as CDT and DITO, relatively little attention has been paid to the geometric quantities of this model. The geometric quantities, which are robust against certain types of noise and errors, have the potential to be powerful tools for quantum computation and quantum information processing. Therefore, our work not only investigates the properties of geometric quantities of the asymmetric

*zglv@sjtu.edu.cn

semiclassical Rabi model but also provides insights into the behavior in a wide range of parameter space.

In this work we investigate the harmonic resonance of the AA phase and the time-energy uncertainty of the asymmetric semiclassical Rabi model, which is beyond the work on the unbiased case [58]. First, we generalize the harmonic resonance features of both geometric quantities in parameter space and further explore the feature of the harmonic resonance. To derive the analytical expression for the AA phase, we employ counter-rotating hybridized rotating-wave (CHRW) method, which takes account of the influences of counter-rotating terms and bias together and is more reliable than the rotating-wave approximation (RWA). Further, considering the second harmonic terms of the Hamiltonian in the rotating frame, we combine perturbation theory with the CHRW method to calculate the AA phase and reveal its subtle resonant picture. Interestingly, at certain points in the parameter space, the odd harmonic resonance disappears in the numerical results. Using Floquet theory [39,59], we explain this interesting phenomenon and reveal the relation between the hidden symmetry of the asymmetric semiclassical Rabi model and odd harmonic resonance. While the hidden symmetry of the asymmetric quantum Rabi model has been extensively studied, our results provide the first instructive evidence for the similar phenomenon in the semiclassical counterpart.

The structure of this work is as follows. In Sec. II, after a brief review of both geometric quantities, we perform numerical calculations to demonstrate the resonance phenomenon and show the features of harmonic resonance. In Sec. III we employ the CHRW method to analytically calculate the AA phase and the positions of the higher-order harmonic resonances. In Sec. IV we apply perturbation theory based on the CHRW method to take into account the effects of higher-order harmonic terms in calculating the AA phase in the higher-order harmonic resonance regime. In Sec. V we shed light on the absence of harmonic resonance in the results of numerical calculation as hidden symmetry appears. This is further discussed through comparison between the asymmetric semiclassical Rabi model and the asymmetric quantum Rabi model. Finally, we give the conclusion of this paper in Sec. VI.

II. RESONANCE OF AHARONOV-ANANDAN PHASE AND TIME-ENERGY UNCERTAINTY

The Hamiltonian of the asymmetric semiclassical Rabi model reads

$$H(t) = -\frac{\Delta}{2}\sigma_x - \frac{\epsilon + A\cos(\omega t)}{2}\sigma_z, \qquad (1)$$

where σ_x and σ_z are the Pauli matrices, Δ is the tunneling strength, and ϵ is the static bias. A, ω, and $T = 2\pi/\omega$ are the amplitude, frequency, and period of the driving field, respectively. We set $\hbar = 1$ throughout this paper and also use $\varepsilon(t) = \epsilon + A\cos(\omega t)$ to denote the bias-modulated driving field [44,56,60]. This Hamiltonian can represent the systems moving in an effective double-well potential modulated by an ac field, under the condition that only the ground state in either well can be occupied [56,61]. A system initially localized in one well will oscillate between the eigenstates in the left

and right well due to quantum mechanical tunneling, which is exemplified by the two equivalent configurations of NH_3, as well as the two current states of a flux qubit [55,60].

By implementing a rotation about the y axis on this Hamiltonian, we obtain a transformed representation $\exp(i\pi\sigma_y/4)H(t)\exp(-i\pi\sigma_y/4) = -\frac{\Delta}{2}\sigma_z + \frac{\epsilon + A\cos(\omega t)}{2}\sigma_x$. This particular form of the Hamiltonian is prevalently employed in the fields of quantum optics and nuclear magnetic resonance, where Δ signifies the energy difference between the two levels, and the driving term causes transitions between these levels [62,63].

In the following we first present a succinct overview of the concepts and geometric properties of the AA phase and the time-energy uncertainty in Secs. II A and II B. Then we display the Δ dependence of both geometric quantities using numerical methods in Sec. II C and further discuss the features of resonance in Sec. II D.

A. Aharonov-Anandan phase

Since the AA phase is a generalization of Berry phase, it is pertinent to briefly review the fundamental concepts and geometric properties of Berry's phase. Consider a time-dependent Hamiltonian $H(\mathbf{R}(t))$, where $\mathbf{R} = (R_1, R_2, ..., R_n)$ and $\mathbf{R}(T) = \mathbf{R}(0)$, with the initial state being the mth eigenstate $|m(0)\rangle$ of $H(\mathbf{R}(0))$. If the system is subjected to adiabatic processes, i.e., $|\langle j|\partial H/\partial t|k\rangle| \ll (E_j - E_k)^2$, $(j \neq k)$, where E_j is the jth eigenenergy of $H(\mathbf{R}(t))$, the state of the system will remain in the mth eigenstate $|m(t)\rangle$ while also obtaining a phase factor $\exp[i(\alpha_m(t) + \gamma_m(t)]$, where $\alpha_m(t) = -\int_0^t E_m(t')dt'$ is called the dynamical phase, and $\gamma_m(t) = i\int_0^t \langle m(t')|\dot{m}(t')\rangle dt'$ is called the adiabatic phase. Berry's phase is defined as the adiabatic phase acquired over a cycle, i.e.,$\gamma_m(T)$, which has been proved to be real and measurable.

The geometric property of Berry's phase corresponds to its relation to the solid angle subtended by the closed path in the parameter space spanned by $\mathbf{R}$ [1]. Consequently, it is referred to as the geometric phase.

Based on Berry's phase, AA removed the adiabatic restriction, while assuming that the initial and final states of the quantum system differ by a total phase factor $e^{i\theta}$ [13]. Since the Hamiltonian in Eq. (1) is periodic, the cyclic state $|\psi(t)\rangle$ satisfies

$$|\psi(T)\rangle = e^{i\theta}|\psi(0)\rangle, \qquad (2)$$

where θ and $|\psi(0)\rangle$ are defined as the total phase and the cyclic initial state, respectively. Then the AA phase is defined by subtracting the dynamical phase α from θ [13]:

$$\gamma = \theta - \alpha, \qquad (3)$$

where the dynamical phase is calculated by

$$\alpha = -\int_0^T \langle\psi|H|\psi\rangle d\tau. \qquad (4)$$

The geometric property of AA phase is embodied in the projective Hilbert space $\mathcal{P}$ (see Appendix A), in which the curve $\mathcal{C}$ traversed by the system decides the value of AA phase. Quantities with such property are referred to as geometric quantities by AA.
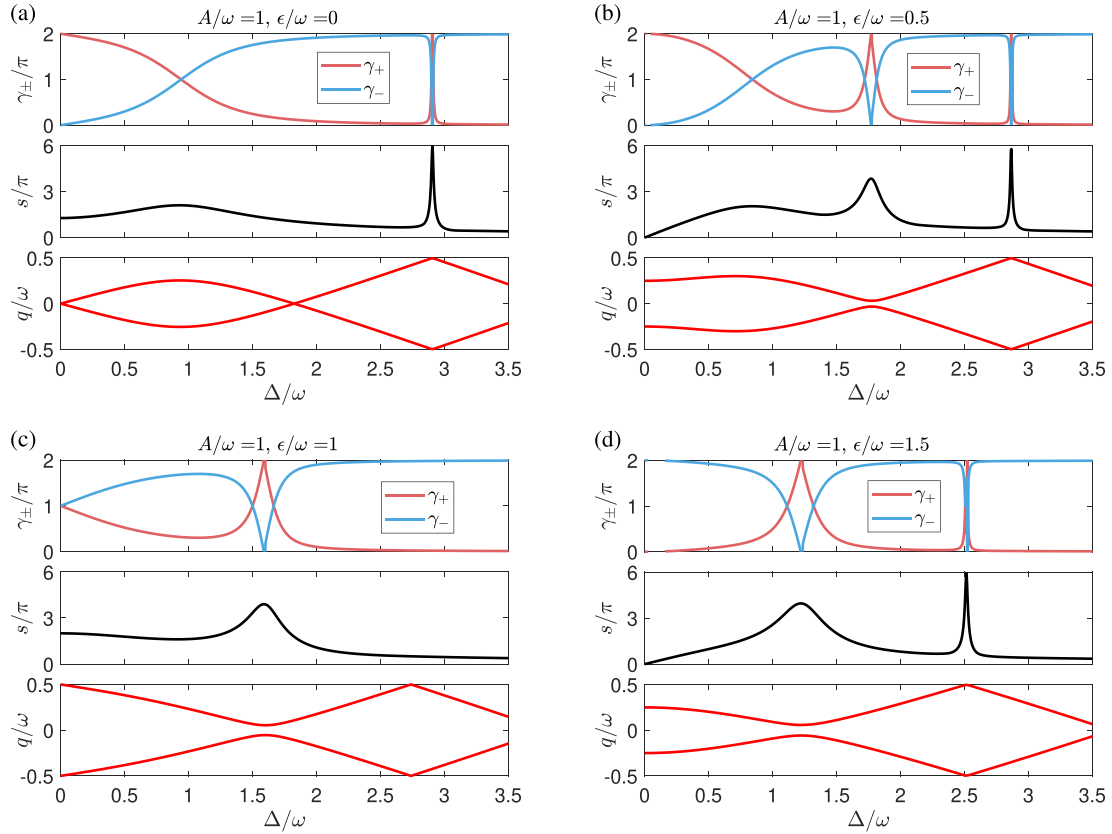
FIG. 1. AA phases $\gamma_\pm$, time-energy uncertainty s, and quasienergy q (see Appendix B 1) as a function of Δ/ω for different values of ϵ/ω with a fixed driving strength $A/\omega = 1$. (a) $\epsilon/\omega = 0$. (b) $\epsilon/\omega = 0.5$. (c) $\epsilon/\omega = 1$. (d) $\epsilon/\omega = 1.5$. γ_+ and γ_- are AA phases corresponding to different cyclic initial states, and we set here $\gamma_- \equiv 2\pi - \gamma_+$ according to the complementary relation. $\gamma_\pm$ and s are all divided by π, and q is divided by ω in the figures. We have selected the interval $[0, 2\pi]$ as the principal value range for the AA phase.

B. Time-energy uncertainty

Another geometric quantity under discussion is the time-energy uncertainty, defined as the time integral of the standard of energy:

$$s = 2 \int \frac{\Delta E(t)}{\hbar} dt, \qquad (5)$$

where

$$\Delta E(t) = [\langle \psi | H^2 | \psi \rangle - \langle \psi | H | \psi \rangle^2]^{1/2}. \qquad (6)$$

The coefficients in Eq. (5) enable s to be equivalent to the distance of curve $\mathcal{C}$ along which the state evolves in projective Hilbert space $\mathcal{P}$, measured by the Fubini-Study metric [19]. Owing to the periodicity of the Hamiltonian in Eq. (1), the curve $\mathcal{C}$ will overlap beyond a single period. As such, it is adequate to compute the time-energy uncertainty within one period.

Suppose that $|\psi\rangle$ and $|\psi + d\psi\rangle$ are separated by an infinitesimal distance. Then the following expression for an infinitesimal length of path ds traversed by the state vector can be derived:

$$ds^2 = 4(1 - |\langle \psi | \psi + d\psi \rangle^2|). \qquad (7)$$

The projective Hilbert space for a two-level system can be identified as the Bloch sphere. In the present case, the Fubini-Study metric is the usual metric on the Bloch sphere with unit radius. Therefore ds can also be obtained as

$$ds = d\phi, \qquad (8)$$

where ϕ is the angle between $|\psi\rangle$ and $|\psi + d\psi\rangle$. The equivalence of Eqs. (7) and (8) can also be easily verified by means of numerical calculation.

C. Numerical results

We present the Δ dependence of the AA phase, the time-energy uncertainty, and the quasienergy (see Appendix B 1) for different biases using numerical methods in Fig. 1. With the Hamiltonian in Eq. (1), we first numerically solve the Schrödinger equation to obtain the evolution operator $U(t)$:

$$i\partial_t U(t) = H(t)U(t). \qquad (9)$$

Then both the total phase θ and the cyclic initial state $|\psi(0)\rangle$ can be obtained from the eigenvalues and eigenvectors of $U(t = T)$. Finally, through numerical integration we can calculate the AA phase using Eqs. (3) and (4), and the time-energy uncertainty using Eqs. (5) and (6). On the other hand, the quasienergy is obtained by diagonalizing the Floquet Hamiltonian numerically, which we will discuss in detail in Sec. V.

For the semiclassical Rabi model, we obtain AA phases $\gamma_\pm$ which correspond to different cyclic initial states and satisfy $\gamma_+ + \gamma_- = 2l\pi, l \in \mathbb{Z}$ (see Appendix B). Nevertheless,
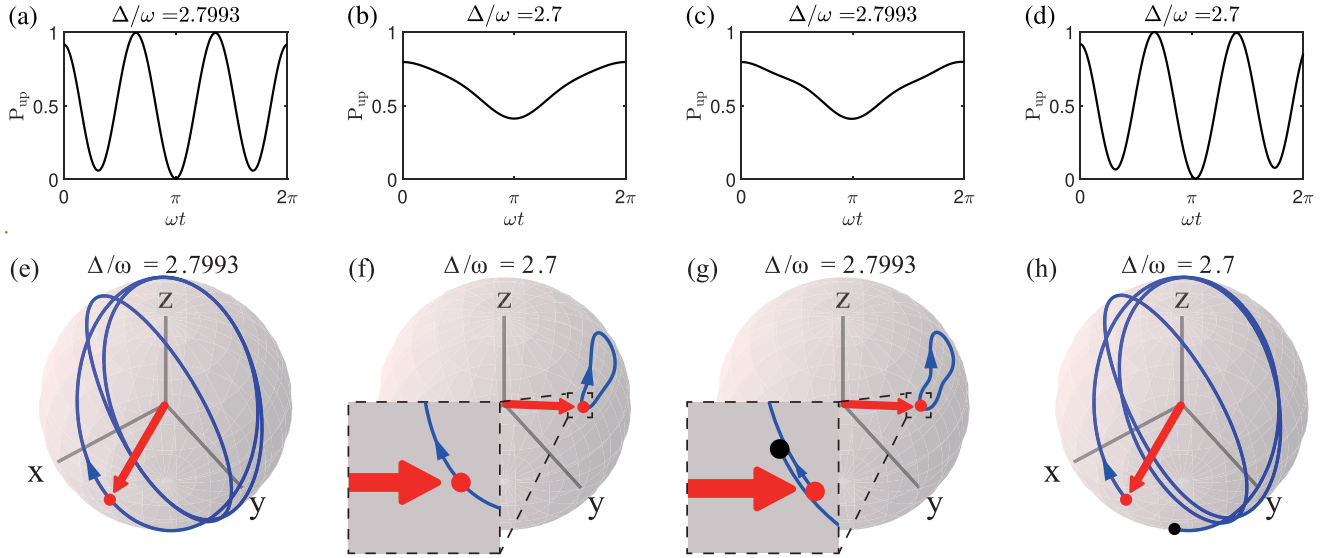
FIG. 2. (a–d) Time evolution of $P_{\rm up}$ for different tunneling strength Δ/ω and initial states, with $A/\omega = 1$ and $\epsilon/\omega = 0.8$ fixed: (a) $\Delta/\omega = 2.7993$ and the initial state is $|\psi_{\rm res}(0)\rangle$; (b) $\Delta/\omega = 2.7$ and the initial state is $|\psi(0)\rangle|_{\Delta/\omega=2.7}$; (c) $\Delta/\omega = 2.7993$ and the initial state is $|\psi(0)\rangle|_{\Delta/\omega=2.7}$; (d) $\Delta/\omega = 2.7$ and the initial state is $|\psi_{\rm res}(0)\rangle$. (e–h) Trajectories on the Bloch sphere with the parameters and the initial states corresponding to (a–d), respectively. The red arrows and dots on the Bloch spheres represent the initial states, while the black dots label the final states. The arrows on the trajectories represent the directions of quantum state evolution. In (f) and (g), we zoom in on the divergence and the convergence of the initial and the final states, respectively.

the values of their time-energy uncertainty are equal, which means their trajectories in the projective Hilbert space are identical. Note that we have selected the interval $[0, 2\pi]$ as the principal value range for the AA phase and set $\gamma_+ + \gamma_- = 2\pi$.

We show the characters of the resonance from the three quantities: AA phases $\gamma_\pm$, time-energy uncertainty s, and quasienergy q. The resonance feature of the time-energy uncertainty is quite pronounced. At the harmonic resonance, the uncertainty reaches its local maxima, which are close to $2\pi, 4\pi$, and 6π for the main, second, and third resonance, respectively. Meanwhile, in the vicinity of the harmonic resonance corresponding to the uncertainty, both branches of the AA phase $\gamma_\pm$ pass through $\gamma = \pi$, and the number of intersections increases with the order of resonance. At the same time, the branches of quasienergy exhibit avoided crossing. Through numerical calculations we have found that the harmonic resonance of the three quantities tends to coincide.

In the top and middle panels of Fig. 1(a) we display the geometric quantities for the Rabi model without bias, i.e., $\epsilon = 0$. In this case only the main and third harmonic resonance occur at $\Delta/\omega \approx 1$ and $\Delta/\omega \approx 3$, respectively. Near these resonances, γ_+ (or γ_-) passes through π once and more than once, respectively. In the bottom panel of Fig. 1(a), the quasienergy spectrum near the main and third harmonic resonance regime exhibits anticrossing, but that near $\Delta/\omega = 2$ exhibits crossing, which indicates the corresponding relation between geometric quantities and quasienergy spectra.

When $\epsilon/\omega > 0$, the second harmonic resonance contributed by the bias term at $\Delta/\omega \approx 2$ occurs, besides the main and third harmonic resonances, as observed in Fig. 1(b). With the increase of ϵ/ω, all the resonance shifts toward smaller values of Δ/ω, and the main harmonic resonance eventually vanishes as $\epsilon/\omega \geqslant 1$, as shown in Figs. 1(c) and 1(d). When $\epsilon/\omega = 1$, the third harmonic resonance also disappears,

because both geometric quantities are relevant to the hidden symmetry of the asymmetric semiclassical Rabi model, which we will come back to discuss in Sec. V.

D. Features of resonance

To explore the condition of resonance and visualize its features, in Fig. 2 we demonstrate the population dynamics of the Rabi model and trajectories on the Bloch sphere for different tunneling strengths Δ/ω and initial states. For $A/\omega = 1$ and $\epsilon/\omega = 0.8$, the third harmonic resonance happens at $\Delta/\omega = 2.7993$, and we use $|\psi(0)\rangle \equiv |\psi_{\rm res}(0)\rangle$ to denote one of its cyclic initial states, while at the near-resonance position $\Delta/\omega = 2.7$, one of its cyclic initial states is denoted as $|\psi(0)\rangle|_{\Delta/\omega=2.7}$. Figures 2(a)–2(d) show the population of the spin-up state $[1 \quad 0]^T$ in the σ_z basis as a function of t for different cases, calculated by

$$P_{\rm up}(t) = \overline{\frac{\sigma_z(t) + 1}{2}} = \langle\psi(0)|U(t)^\dagger \frac{\sigma_z + 1}{2} U(t)|\psi(0)\rangle, \quad (10)$$

which represents the dynamics of the two-level systems. Figures 2(e)–2(h) show the corresponding trajectories of $|\psi(t)\rangle = U(t)|\psi(0)\rangle$ on the Bloch sphere, with red dots labeling the initial states and black dots labeling the final states.

In Figs. 2(a) and 2(e), $\Delta/\omega = 2.7993$, which is the resonance position, and the initial state is $|\psi_{\rm res}(0)\rangle$. The features of resonance are manifestly shown by the rapid oscillation of $P_{\rm up}$ and the trajectory on the Bloch sphere whose length is very close to 6π. As seen in Fig. 2(e), the initial and final states converge, because the initial state is the cyclic initial state for $\Delta/\omega = 2.7993$. In Figs. 2(b) and 2(f), $\Delta/\omega = 2.7$, which is corresponding to the nonresonance position, and the initial state is $|\psi(0)\rangle|_{\Delta/\omega=2.7}$. In this case resonance is not observed, as $P_{\rm up}$ varies slowly and the trajectory greatly contracts.

In Figs. 2(c) and 2(g), we show the population dynamics and the trajectory on the Bloch sphere for $\Delta/\omega = 2.7993$ initially prepared from the initial cyclic state with $|\psi(0)\rangle|_{\Delta/\omega=2.7}$, respectively. We find that the dynamics and trajectory on the Bloch sphere in this case are similar to those results in Figs. 2(b) and 2(f), indicating that resonance disappears. In Figs. 2(d) and 2(h), if the initial state is initially prepared as $|\psi_{\text{res}}(0)\rangle$ and a nonresonant parameter $\Delta/\omega = 2.7$ is set, it is found that like-resonance phenomena recur, which seems similar to those in Figs. 2(a) and 2(e). Note that the initial and final states diverge in Figs. 2(g) and 2(h), because in both cases the initial states and the parameters Δ/ω do not match.

From Fig. 2 we conclude that harmonic resonance mainly comes from the initial state $|\psi(0)\rangle$. As long as one cyclic initial state corresponding to its resonance position is selected, like-resonance phenomena can happen even if the parameter Δ/ω does not match that of the resonance. Meanwhile, $|\psi(0)\rangle$ is highly sensitive to Δ/ω in the vicinity of harmonic resonance, as is observed from Figs. 2(e) and 2(g).

III. COUNTER-ROTATING HYBRIDIZED ROTATING-WAVE METHOD

In this section we apply the CHRW method to analytically calculate the AA phase of the asymmetric semiclassical Rabi model. We first introduce the CHRW methodology in Sec. III A and then present the analytical expression for the AA phase in Sec. III B. Finally, we calculate the positions of the higher-order harmonic resonances by the CHRW method in Sec. III C.

A. Methodology

We perform the unitary transformation with a generator $S(t) = -i\frac{A}{2\omega}\sin(\omega t)(\xi\sigma_z + \zeta\sigma_x)$ to the Hamiltonian in Eq. (1). The two parameters ξ and ζ are determined later. In the rotating frame we obtain the evolution operator

$$i\frac{dU'(t)}{dt} = H'(t)U'(t), \tag{11}$$

in which $U'(t) = e^{S(t)}U(t)$ and $H'(t) = e^{S(t)}H(t)e^{-S(t)} - ie^{S(t)}\partial_t e^{-S(t)}$. Then the wave function is obtained $|\psi'(t)\rangle = e^{S(t)}|\psi\rangle$, and the transformed Hamiltonian is written

$$H' = -\frac{\Delta}{2}\left[\sigma_x - \frac{1-\cos\Theta}{x^2}\xi(\xi\sigma_x - \zeta\sigma_z) + \frac{\sin\Theta}{x}\xi\sigma_y\right]$$
$$- \frac{\varepsilon(t)}{2}\left[\sigma_z + \frac{1-\cos\Theta}{x^2}\zeta(\xi\sigma_x - \zeta\sigma_z) - \frac{\sin\Theta}{x}\zeta\sigma_y\right]$$
$$+ \frac{A}{2}(\xi\sigma_z + \zeta\sigma_x)\cos(\omega t), \tag{12}$$

where $\Theta = z\sin(\omega t)$, $z = \frac{A}{\omega}x$, and $x = \sqrt{\xi^2 + \zeta^2}$. After using the identity

$$\exp(iy\sin\alpha) = \sum_{-\infty}^{\infty}J_n(y)e^{in\alpha}, \tag{13}$$

where $J_n(y)$ are the nth-order Bessel functions of the first kind, and we divide the Hamiltonian into four parts according to the order of the harmonics,

$$H' = H_0' + H_1'(t) + H_2'(t) + V(t), \tag{14}$$

where

$$H_0' = -\frac{\tilde{\Delta}}{2}\sigma_x - \frac{\tilde{\epsilon}}{2}\sigma_z, \tag{15}$$

$$H_1' = -\frac{(\Delta\xi - \epsilon\zeta)}{x}J_1(z)\sin(\omega t)\sigma_y - \frac{A}{2}[1 - \xi - \zeta^2 j_c]$$
$$\times\cos(\omega t)\sigma_z + \frac{A}{2}\zeta[1 - \xi j_c]\cos(\omega t)\sigma_x, \tag{16}$$

$$H_2' = \frac{A}{2}\frac{\zeta}{x}J_1(z)\sin(2\omega t)\sigma_y$$
$$- \frac{(\Delta\xi - \epsilon\zeta)}{x^2}J_2(z)\cos(2\omega t)(\xi\sigma_x - \zeta\sigma_z), \tag{17}$$

$$V = \frac{A}{2}\frac{\zeta}{x^2}J_2(z)\cos(3\omega t)(\xi\sigma_x - \zeta\sigma_z) - \frac{[\Delta\xi - \varepsilon(t)\zeta]}{x^2}$$
$$\times\sum_{n=2}^{\infty}\{xJ_{2n-1}(z)\sin[(2n-1)\omega t]\sigma_y$$
$$+ J_{2n}(z)\cos(2n\omega t)(\xi\sigma_x - \zeta\sigma_z)\}. \tag{18}$$

The parameters $\tilde{\Delta}, \tilde{\epsilon}$ and j_c are defined as

$$\tilde{\epsilon} = \epsilon + \frac{\zeta}{x^2}[1 - J_0(z)](\Delta\xi - \epsilon\zeta), \tag{19}$$

$$\tilde{\Delta} = \Delta - \frac{\xi}{x^2}[1 - J_0(z)](\Delta\xi - \epsilon\zeta), \tag{20}$$

$$j_c = \frac{1 - J_0(z) - J_2(z)}{x^2}, \tag{21}$$

respectively. Note that the zero-ω Hamiltonian H_0' consists of the renormalized tunneling term and renormalized bias one, the single-ω Hamiltonian H_1' corresponds to single-harmonic processes, and the double-ω Hamiltonian H_2' specifies second-order harmonic processes. Finally, $V(t)$ includes all higher-order harmonic terms $n\omega, n \geq 3$. Until now, no approximations are made, and the effects of the counter-rotating terms and bias are all taken into account. Next, we keep all the zeroth and first harmonics of the transformed Hamiltonian ($n\omega, n = 0, 1$), i.e., $H' \approx H_0' + H_1'$, and neglect the higher-order harmonic terms that involve all multi-ω or multiphoton assisted transitions ($n\omega, n = 2, 3, 4, ...$). The validity of the omission of $H_2' + V$ depends on the effects of the higher-frequency driving terms whose contribution to the dynamics is not prominent except for the ultrastrong driving-strength case [57].

The Hamiltonian H_0' is diagonalized by a unitary matrix $D = u\sigma_z - v\sigma_x$ with $u = \sqrt{\frac{1}{2} - \frac{\tilde{\epsilon}}{2\tilde{\Xi}}}$ and $v = \sqrt{\frac{1}{2} + \frac{\tilde{\epsilon}}{2\tilde{\Xi}}}$ to the form

$$\tilde{H}_0 = \frac{\tilde{\Xi}}{2}\tau_z, \tag{22}$$

where $\tilde{\Xi} = \sqrt{\tilde{\Delta}^2 + \tilde{\epsilon}^2}$ is the renormalized energy splitting, τ_z is the z-component pseudospin operator in the energy eigenbasis.

The Hamiltonian H_1' is then changed to

$$
\begin{aligned}
\tilde{H}_1 &= D^\dagger H_1' D \\
&= \frac{(\Delta\xi - \epsilon\zeta)}{x} J_1(z) \sin(\omega t)\tau_y \\
&\quad + \frac{A}{2}[1 - \xi - \zeta^2 j_c] \cos(\omega t)\left(\frac{\tilde{\epsilon}}{\tilde{\Xi}}\tau_z + \frac{\tilde{\Delta}}{\tilde{\Xi}}\tau_x\right) \\
&\quad + \frac{A}{2}\zeta[1 - \xi j_c] \cos(\omega t)\left(\frac{\tilde{\epsilon}}{\tilde{\Xi}}\tau_x - \frac{\tilde{\Delta}}{\tilde{\Xi}}\tau_z\right),
\end{aligned}
\tag{23}
$$

where τ_x and τ_y are, respectively, the x component and the y component spin operators in the energy eigenbasis. In order to make the driving interaction term $D^\dagger H_1' D$ hold the RWA-like form, we choose the two proper parameters ξ and ζ to satisfy the following two self-consistent equations:

$$
0 = \frac{A}{2}\left[\frac{\tilde{\Delta}}{\tilde{\Xi}}(1 - \xi - \zeta^2 j_c) + \frac{\tilde{\epsilon}}{\tilde{\Xi}}\zeta(1 - \xi j_c)\right] - \frac{\Delta\xi - \epsilon\zeta}{x}J_1(z),
\tag{24}
$$

$$
0 = \tilde{\epsilon}(1 - \xi - \zeta^2 j_c) - \tilde{\Delta}\zeta(1 - \xi j_c).
\tag{25}
$$

Therefore we obtain

$$
\begin{aligned}
\tilde{H} &= D^\dagger(H_0' + H_1')D \\
&= \frac{\tilde{\Xi}}{2}\tau_z + \frac{\tilde{A}}{2}[\tau_+ \exp(-i\omega t) + \tau_- \exp(i\omega t)],
\end{aligned}
\tag{26}
$$

where $\tau_\pm = (\tau_x \pm i\tau_y)/2$, and $\tilde{A}$ is the renormalized amplitude of the driving field resulting from the combination of the counter-rotating coupling and static bias,

$$
\tilde{A} = \frac{\Delta\xi - \epsilon\zeta}{x}2J_1(z).
\tag{27}
$$

B. Aharonov-Anandan phase

The solutions to the Schrödinger equation corresponding to $\tilde{H}$ are denoted as $|\tilde{\psi}\rangle$ and satisfy $|\tilde{\psi}\rangle = D^\dagger|\psi'\rangle = D^\dagger e^S|\psi\rangle$. Meanwhile, the evolution operator $\tilde{U}(t)$ corresponding to $\tilde{H}$ is solved analytically,

$$
\tilde{U}(t) = \begin{bmatrix} e^{-i\frac{\omega t}{2}}\left[\cos\left(\frac{\tilde{\Omega}t}{2}\right) - \frac{i\tilde{\delta}}{\tilde{\Omega}}\sin\left(\frac{\tilde{\Omega}t}{2}\right)\right] & -e^{-i\frac{\omega t}{2}}\frac{i\tilde{A}}{\tilde{\Omega}}\sin\left(\frac{\tilde{\Omega}t}{2}\right) \\ -e^{i\frac{\omega t}{2}}\frac{i\tilde{A}}{\tilde{\Omega}}\sin\left(\frac{\tilde{\Omega}t}{2}\right) & e^{i\frac{\omega t}{2}}\left[\cos\left(\frac{\tilde{\Omega}t}{2}\right) + \frac{i\tilde{\delta}}{\tilde{\Omega}}\sin\left(\frac{\tilde{\Omega}t}{2}\right)\right] \end{bmatrix},
\tag{28}
$$

where $\tilde{\Omega} = \sqrt{\tilde{\delta}^2 + \tilde{A}^2}$ and $\tilde{\delta} = \tilde{\Xi} - \omega$ are, respectively, the modulated Rabi frequency and the renormalized detuning parameter given by the CHRW method.

By the analytical expression of the transformed evolution operator $\tilde{U}(t)$, we calculate the cyclic states $|\psi_\pm(t)\rangle$ by

$$
|\psi_\pm(t)\rangle = e^{-S(t)}D|\tilde{\psi}_\pm(t)\rangle = e^{-S(t)}D\tilde{U}(t)|\tilde{\psi}_\pm(0)\rangle
\tag{29}
$$

and total phases $\theta_\pm$ by their eigenvalues $e^{i\theta_\pm}$. The dynamical phases are obtained:

$$
\begin{aligned}
\alpha_\pm &= -\int_0^T \langle\psi_\pm|H|\psi_\pm\rangle d\tau \\
&= -\int_0^T \langle\tilde{\psi}_\pm(0)|\tilde{U}^\dagger D^\dagger e^S H e^{-S} D\tilde{U}|\tilde{\psi}_\pm(0)\rangle d\tau.
\end{aligned}
\tag{30}
$$

By $\tilde{U}(T)$ in Eq. (28),

$$
\tilde{U}(T) = -\cos\left(\frac{\tilde{\Omega}T}{2}\right)I + i\frac{\tilde{A}}{\tilde{\Omega}}\sin\left(\frac{\tilde{\Omega}T}{2}\right)\tau_x + i\frac{\tilde{\delta}}{\tilde{\Omega}}\sin\left(\frac{\tilde{\Omega}T}{2}\right)\tau_z,
\tag{31}
$$

we get its eigenvectors and phases of eigenvalues

$$
|\tilde{\psi}_\pm(0)\rangle = \sqrt{\frac{2\tilde{\Omega}}{\tilde{\Omega} \mp \tilde{\delta}}}\begin{pmatrix} \frac{1}{2} \mp \frac{\tilde{\delta}}{2\tilde{\Omega}} \\ \mp \frac{\tilde{A}}{2\tilde{\Omega}} \end{pmatrix},
\tag{32}
$$

$$
\theta_\pm = \pm\frac{\tilde{\Omega} - \omega}{2}T,
\tag{33}
$$

respectively. The dynamic phases read

$$
\begin{aligned}
\alpha_\pm = \pm\frac{T}{4\tilde{\Omega}}\Bigg\{&\epsilon\Bigg[\frac{\tilde{\epsilon}}{\tilde{\Xi}}\tilde{\delta}(1 + J_0(z)) + \frac{2\xi\zeta}{x^2}\frac{\tilde{\Delta}}{\tilde{\Xi}}\tilde{\delta}(1 - J_0(z)) - \frac{2\zeta}{x}\tilde{A}J_1(z) + \frac{\xi^2 - \zeta^2}{x^2}\frac{\tilde{\epsilon}}{\tilde{\Xi}}\tilde{\delta}(1 - J_0(z))\Bigg] \\
&+ A\tilde{A}\Bigg[\frac{\xi^2}{x^2}\frac{\tilde{\Delta}}{\tilde{\Xi}} + \frac{\xi\zeta}{x^2}\frac{\tilde{\epsilon}}{\tilde{\Xi}}\left(\frac{2J_1(z)}{z} - 1\right) + \frac{2\zeta^2}{x^2}\frac{\tilde{\Delta}}{\tilde{\Xi}}\frac{J_1(z)}{z}\Bigg] + 2\Delta\Bigg[\frac{\zeta^2}{x^2}\frac{\tilde{\Delta}}{\tilde{\Xi}}\tilde{\delta} + \frac{\xi^2}{x^2}\frac{\tilde{\Delta}}{\tilde{\Xi}}J_0(z)\tilde{\delta} + \frac{\xi\zeta}{x^2}\frac{\tilde{\epsilon}}{\tilde{\Xi}}\tilde{\delta}(1 - J_0(z)) + \frac{\xi}{x}\tilde{A}J_1(z)\Bigg]\Bigg\}.
\end{aligned}
\tag{34}
$$

Finally we obtain the analytical expression of AA phases:

$$\gamma_\pm = \theta_\pm - \alpha_\pm$$

$$= \pm \frac{T}{4\tilde{\Omega}}\left\{ 2\tilde{\Omega}(\tilde{\Omega} - \omega) - \epsilon\left[\frac{\tilde{\epsilon}}{\tilde{\Xi}}\tilde{\delta}(1 + J_0(z)) + \frac{2\xi\zeta}{x^2}\frac{\tilde{\Delta}}{\tilde{\Xi}}\tilde{\delta}(1 - J_0(z)) - \frac{2\zeta}{x}\tilde{A}J_1(z) + \frac{\xi^2 - \zeta^2}{x^2}\frac{\tilde{\epsilon}}{\tilde{\Xi}}\tilde{\delta}(1 - J_0(z)) \right] - A\tilde{A} \right.$$

$$\left[\frac{\xi^2}{x^2}\frac{\tilde{\Delta}}{\tilde{\Xi}} + \frac{\xi\zeta}{x^2}\frac{\tilde{\epsilon}}{\tilde{\Xi}}\left(\frac{2J_1(z)}{z} - 1 \right) + \frac{2\zeta^2}{x^2}\frac{\tilde{\Delta}}{\tilde{\Xi}}\frac{J_1(z)}{z} \right] - 2\Delta\left[\frac{\zeta^2}{x^2}\frac{\tilde{\Delta}}{\tilde{\Xi}}\tilde{\delta} + \frac{\xi^2}{x^2}\frac{\tilde{\Delta}}{\tilde{\Xi}}J_0(z)\tilde{\delta} + \frac{\xi\zeta}{x^2}\frac{\tilde{\epsilon}}{\tilde{\Xi}}\tilde{\delta}(1 - J_0(z)) + \frac{\xi}{x}\tilde{A}J_1(z) \right] \left. \right\}. \quad (35)$$

For the symmetric case, i.e., $\epsilon = 0$, the result of the parameter $\zeta = 0$ is self-consistently solved by Eqs. (24) and (25). This simplifies Eq. (35) to the previous result derived in [58], albeit with slight differences in the coefficients due to the present definition of $\tilde{A}$:

$$\gamma_\pm = \pm\left[\frac{\tilde{\Omega} - \omega}{2} - \frac{\tilde{A}}{2\tilde{\Omega}}\left(\frac{\tilde{\Delta}\tilde{\delta}}{\tilde{A}} + \frac{A}{2} + \frac{\tilde{A}}{2} \right) \right]T. \quad (36)$$

C. Positions of the harmonic resonance

By the Rabi frequency of the CHRW method, we calculate the positions of the higher-order harmonic resonance [58]. The second harmonic resonance occurs when the modulated effective Rabi frequency equals the frequency of external driving field, i.e.,

$$\tilde{\Omega} = \omega. \quad (37)$$

Likewise, the condition for the third harmonic resonance is

$$\tilde{\Omega} = 2\omega. \quad (38)$$

An analytical expression for the Rabi frequency up to the second order in the driving strength A is derived in Ref. [57]:

$$\tilde{\Omega}_{2nd} = (\omega - \Xi_0)^2 + \frac{A^2\Delta^2}{2\Xi_0(\omega + \Xi_0)}, \quad (39)$$

where $\Xi_0 = \sqrt{\Delta^2 + \epsilon^2}$. We use the condition $\tilde{\Omega}_{2nd} = \omega$ to estimate the position of the second harmonic resonance. It is obvious to see that in Fig. 3 the positions of the harmonic resonance of numerically exact results agree well with those of the CHRW method. Both the positions of the second harmonic resonance and third harmonic resonance show the tendency of decrease of the tunneling strength as the bias increases, indicating a compensating effect between Δ and ϵ. The result obtained by using $\tilde{\Omega} = \omega$, which is shown by the blue line in Fig. 3(a), is in agreement with the numerically exact solution when $\epsilon < \Delta$, despite a tiny deviation that originates from neglecting higher-order terms of A in deriving Eq. (39). However, the relation $\tilde{\Omega}_{2nd} = 2\omega$ could not correctly predict the third harmonic resonance, because $\tilde{\Omega}_{2nd}$ does not take into account the competition effect of bias and counter-rotating terms in the higher-order resonance parameter regime, such as $\Delta \sim 3\omega$.

IV. PERTURBATION THEORY

Although the CHRW method can predict the positions of the higher-order harmonic resonance of the AA phase and depict its asymptotic tendency as a function of Δ/ω, it is necessary to combine it with perturbation theory in

order to reveal the harmonic resonance features. Consider the time-dependent Hamiltonian $\tilde{H}'$ split into a unperturbed Hamiltonian $\tilde{H}$ and a perturbation with a dimensionless parameter λ representing the order of perturbation,

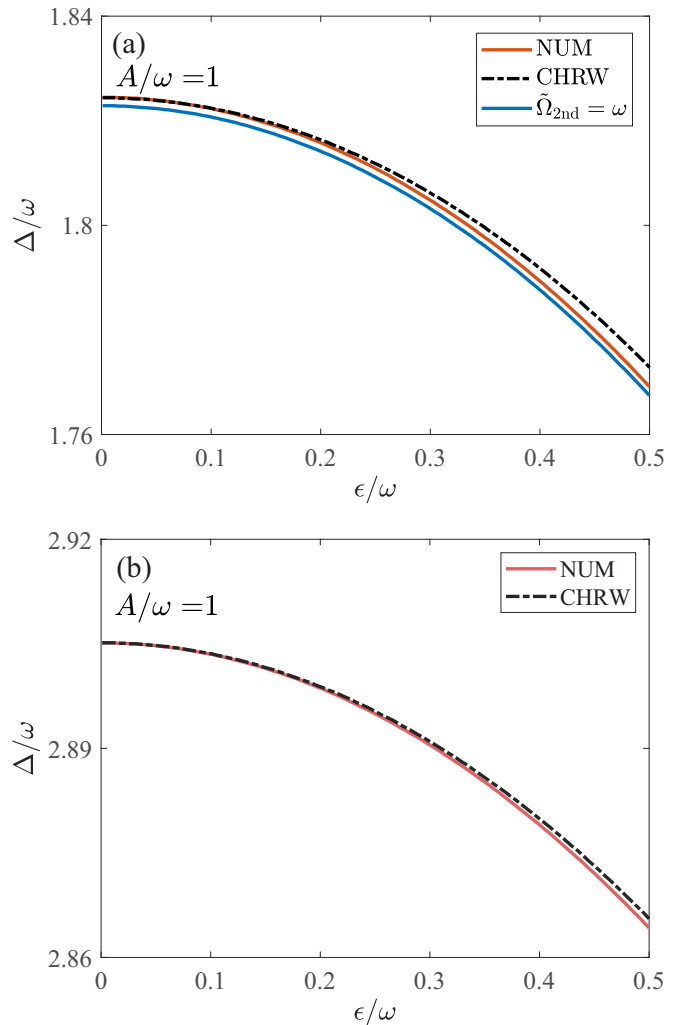$$\tilde{H}' = \tilde{H} + \lambda\tilde{H}_{pt}, \quad (40)$$

FIG. 3. (a) Position of the second harmonic resonance. (b) Position of the third harmonic resonance. $0 < \epsilon/\omega < 0.5$, $A/\omega = 1$ for both figures. The red lines are calculated by the numerically exact method, the dashed dotted lines are obtained by Eqs. (37) and (38) with the CHRW method, and the blue line in (a) is given by $\tilde{\Omega}_{2nd} = \omega$ as an approximation.

and its corresponding time evolution operator

$$\tilde{U}' = \tilde{U} + \lambda \tilde{U}_{pt} + \cdots, \tag{41}$$

where $i\frac{d\tilde{U}}{dt} = \tilde{H}\tilde{U}$. Since $\tilde{U}'(t)$ satisfies the time-dependent Schrödinger equation $i\frac{d\tilde{U}'}{dt} = \tilde{H}'\tilde{U}'$, we can solve $\tilde{U}_{pt}$ to the first order:

$$i\frac{d\tilde{U}_{pt}}{dt} = \tilde{H}\tilde{U}_{pt} + \tilde{H}_{pt}\tilde{U}. \tag{42}$$

Then we analytically solve

$$\tilde{U}_{pt}(t) = -i\tilde{U} \int_0^t \tilde{U}^{-1} \tilde{H}_{pt} \tilde{U} d\tau. \tag{43}$$

In this work we choose the parameter, $A/\omega < 2$, and therefore the influences of second harmonic terms in $H_2'(t)$ are dominant compared with the other higher-harmonic terms in $V(t)$. In the following, by considering the second harmonic terms in H_2',

we calculate the evolution operator under perturbation and then derive modified cyclic initial states and more accurate analytical results for the AA phase. In the energy eigenbasis representation of diagonalization, H_2' becomes

$$\tilde{H}_2 = D^\dagger H_2' D = \tilde{H}_{2y} + \tilde{H}_{2x} + \tilde{H}_{2z}, \tag{44}$$

where

$$\tilde{H}_{2y} = -\frac{A\zeta}{2x} J_1(z) \sin(2\omega t)\tau_y, \tag{45}$$

$$\tilde{H}_{2x} = \frac{\epsilon\zeta - \Delta\xi}{x^2} J_2(z) q \cos(2\omega t)\tau_x, \tag{46}$$

$$\tilde{H}_{2z} = \frac{\epsilon\zeta - \Delta\xi}{x^2} J_2(z) p \cos(2\omega t)\tau_z, \tag{47}$$

and $p = (v^2 - u^2)\zeta - 2\xi uv$ and $q = (v^2 - u^2)\xi + 2uv\zeta$. Here we take into consideration the effects of the terms with τ_x, τ_y, and τ_z separately. First, we explore the effects of $\tilde{H}_{2y}$, calculating the integral:

$$\int_0^T \tilde{U}^{-1} \tilde{H}_{2y} \tilde{U} d\tau = \frac{2A\zeta J_1(z) \sin\left(\frac{\tilde{\Omega}}{2}T\right)}{x\tilde{\Omega}^2(9\omega^4 - 10\omega^2\tilde{\Omega}^2 + \tilde{\Omega}^4)} \left[(3\tilde{\delta}\tilde{\Omega}\omega^3 + 2\tilde{\delta}^2\tilde{\Omega}\omega^2 - \tilde{\delta}\tilde{\Omega}^3\omega) \cos\left(\frac{\tilde{\Omega}}{2}T\right)\tau_x \right.$$

$$\left. + (\tilde{\Omega}^4\omega - 2\tilde{\Omega}^2\tilde{\delta}\omega^2 - 3\tilde{\Omega}^2\omega^3) \sin\left(\frac{\tilde{\Omega}}{2}T\right)\tau_y + \tilde{A}(\tilde{\Omega}^3\omega - 3\tilde{\Omega}\omega^3 - 2\tilde{\Omega}\tilde{\delta}\omega^2) \cos\left(\frac{\tilde{\Omega}}{2}T\right)\tau_z \right]. \tag{48}$$

Substituting Eq. (28) into Eq. (43), we obtain its first-order correction to $\tilde{U}'$:

$$\tilde{U}_{2y}(T) = i\frac{2A\zeta\omega J_1(z) \sin(\frac{\tilde{\Omega}}{2}T)(3\omega + 2\tilde{\delta}\omega - \tilde{\Omega}^2)}{x\tilde{\Omega}(9\omega^4 - 10\omega^2\tilde{\Omega}^2 + \tilde{\Omega}^4)}(\tilde{\delta}\tau_x - \tilde{A}\tau_z). \tag{49}$$

The whole time evolution operator $\tilde{U}_y'(T) = \tilde{U}(T) + \tilde{U}_{2y}(T)$ yields

$$\tilde{U}_y'(T) = -\cos\left(\frac{\tilde{\Omega}T}{2}\right)I + \frac{i}{\tilde{\Omega}} \sin\left(\frac{\tilde{\Omega}T}{2}\right)[(\tilde{A} + k_y\tilde{\delta})\tau_x + (\tilde{\delta} - k_y\tilde{A})\tau_z], \tag{50}$$

where

$$k_y = \frac{2A\zeta\omega J_1(z)(3\omega + 2\tilde{\delta}\omega - \tilde{\Omega}^2)}{x(9\omega^4 - 10\omega^2\tilde{\Omega}^2 + \tilde{\Omega}^4)}. \tag{51}$$

We immediately obtain one of its eigenvectors and its corresponding eigenvalue:

$$|\tilde{\psi}'_{+y}(0)\rangle = \frac{1}{L_y} \begin{bmatrix} \tilde{A} + k_y\tilde{\delta} \\ k_y\tilde{A} - \tilde{\delta} - \sqrt{1 + k_y^2}\tilde{\Omega} \end{bmatrix}, \tag{52}$$

$$\lambda_+ = -\cos\left(\frac{\tilde{\Omega}T}{2}\right) - i\sqrt{1 + k_y^2} \sin\left(\frac{\tilde{\Omega}T}{2}\right), \tag{53}$$

where the normalization factor

$$L_y = \left[2(1 + k_y^2)\tilde{\Omega}^2 - 2(\tilde{\delta} + k_y\tilde{A})\sqrt{1 + k_y^2}\tilde{\Omega}\right]^{1/2}. \tag{54}$$

Because the eigenvalue $|\lambda_+| \simeq 1$, we can regard

$$\theta'_+ = \arg(\lambda_+) = \arctan\left[\sqrt{1 + k_y^2} \tan\left(\frac{\tilde{\Omega}T}{2}\right)\right] - \frac{\omega T}{2} \tag{55}$$

as the modified total phase under perturbation, which includes the effects of counter-rotating terms. Also, the perturbed Rabi frequency in the vicinity of harmonic resonance can be derived accordingly (see Appendix C). In fact, θ'_+ is very close to θ_+ given by the CHRW method, as the eigenvalues of $\tilde{U}_y'(T)$ are very close to those of $\tilde{U}(T)$. Thus we can use the latter to approximate θ'_+, and the less $|k_y|$ is, the better the approximation is.

Owing to the great contribution of $\tilde{U}_{2y}(T)$ to $\tilde{U}'_y(T)$, both the dynamical phase and the AA phase change sharply near higher-order harmonic resonance. Using Eqs. (3) and (30), we obtain the AA phase corresponding to Eq. (52):

$$\gamma_+ = \theta_+ + \int_0^T \langle \tilde{\psi}'_{+y}(0)|\tilde{U}^\dagger D^\dagger e^S H e^{-S} D \tilde{U}|\tilde{\psi}'_{+y}(0)\rangle d\tau. \tag{56}$$

Here we use $\tilde{U}$ instead of $\tilde{U}'$ in the integrand, which causes neglectable difference in the calculation. In light of the complementary relation $\gamma_+ + \gamma_- = 2l\pi, l \in \mathbb{Z}$, we obtain both AA phases approximately as follows:

$$\gamma_\pm \approx \pm \frac{\tilde{\Omega} - \omega}{2}T \mp \frac{\pi}{2L_y^2}\left\{ (\tilde{\delta} + \sqrt{k_y^2 + 1}\tilde{\Omega} - k_y\tilde{A})\left\{ \frac{A^2\tilde{\delta}}{2\omega^3}[\epsilon(\nu^2 - \mu^2) - 2\Delta\mu\nu] - \frac{\tilde{\delta}}{128\omega}(3z^4 - 64z^2 + 512) \right. \right.$$

$$\left. \times (u^2\epsilon - 2uv\Delta - v^2\epsilon) - \frac{2A\tilde{A}}{\omega^2}[(u\epsilon - v\Delta)\nu - (u\Delta + v\epsilon)\mu] + \frac{A\tilde{A}}{\omega}\left[\frac{2}{z}J_1(z) + 1 \right][k_y(u^2 - v^2) + 2uv] \right\}$$

$$\left. + \frac{4k_y}{x^2}J_2(z)(uv - v\mu)\left[k_y\tilde{A}(\tilde{\Omega} + \tilde{\delta}) - (1 + \sqrt{k_y^2 + 1})\tilde{\Omega}\tilde{\delta} - \sqrt{k_y^2 + 1}\tilde{\Omega}^2 - \tilde{\delta}^2 \right] \right\}, \tag{57}$$

where $\mu = \xi u - \zeta v, \nu = \xi v + \zeta u$. The details of derivation are given in Appendix C.

Likewise, when we take account of the influences of $\tilde{H}_{2x}$ and $\tilde{H}_{2z}$, we repeat the processes of derivation above and obtain

$$\tilde{U}_{2x}(T) = \frac{ik_x \sin\left(\frac{\tilde{\Omega}}{2}T \right)}{\tilde{\Omega}}(\tilde{\delta}\tau_x - \tilde{A}\tau_z), \tag{58}$$

$$\tilde{U}_{2z}(T) = \frac{ik_z \sin\left(\frac{\tilde{\Omega}}{2}T \right)}{\tilde{\Omega}}(\tilde{\delta}\tau_x - \tilde{A}\tau_z), \tag{59}$$

where

$$k_x = \frac{2(\Delta\xi - \epsilon\zeta)J_2(z)}{x^2}$$
$$\times \frac{[(v^2 - u^2)\xi + 2uv\zeta](3\omega^3 + 5\omega^2\tilde{\delta} + \omega\tilde{\Omega}^2 - \tilde{\delta}\tilde{\Omega}^2)}{(9\omega^4 - 10\omega^2\tilde{\Omega}^2 + \tilde{\Omega}^4)}, \tag{60}$$

$$k_z = -\frac{2(\Delta\xi - \epsilon\zeta)J_2(z)}{x^2}\frac{\tilde{A}[2\xi uv + \zeta(u^2 - v^2)]}{\tilde{\Omega}^2 - 4\omega^2}. \tag{61}$$

It is noticeable that both $\tilde{U}_{2x}(T)$ and $\tilde{U}_{2z}(T)$ possess a similar mathematical structure to $\tilde{U}_{2y}(T)$ except for their distinct coefficients. If combining them together, we obtain the first-order correction to the time evolution operator $\tilde{U}$. Therefore, it turns out that the same forms of cyclic initial state and dynamical phase as those in Eqs. (52) and (57) remain unchanged. Substituting k_y in Eqs. (54) and (57) with $k = k_y + k_x + k_z$ results in the perturbed result. Moreover, the results are more accurate for the AA phase in comparison with the unperturbed and numerical results, which are shown in Fig. 4. Meanwhile, we can see clearly from Eqs. (51), (60), and (61) that $\tilde{H}_{2y}$ and $\tilde{H}_{2x}$ contribute to the higher-order harmonic resonance for $\tilde{\Omega} \approx \omega$ and $\tilde{\Omega} \approx 3\omega$, while $\tilde{H}_{2z}$ contributes to the higher-order harmonic resonance for $\tilde{\Omega} \approx 2\omega$.

To evaluate the effectiveness of perturbation theory based on the CHRW method, we depict the AA phase γ_+ and the modulated effective Rabi frequency $\tilde{\Omega}$ as a function of Δ/ω in Fig. 4, obtained by the numerical method, the CHRW method, and perturbation theory based on the CHRW method. In Figs. 4(a) and 4(b), we remove the limitation of AA phase

to $[0, 2\pi]$ to better exhibit the harmonic resonance peaks of AA phase. It is obvious to see that the results obtained by the CHRW method exhibit an asymptotic tendency for both the AA phase and the modulated effective Rabi frequency. In contrast, the combination of perturbation theory and the CHRW method (denoted as CHRW+PT) accurately depicts the harmonic resonance peaks of γ_+ and sudden changes of $\tilde{\Omega}$ in the second- and the third-harmonic resonance regimes, defined as the full width at half maximum (FWHM) of AA phase [58]. In Figs. 4(a) and 4(b) we observe not only the third harmonic resonance driven by the external field, but also the second harmonic resonance arising from the combination of bias and driving field. It is known that the odd higher-order harmonic resonance happens in the symmetric Rabi model. However, the asymmetry in the asymmetric Rabi model induces even higher-order harmonic resonance, which is a significant character in the asymmetric Rabi model, compared with the results of the symmetric Rabi model [58]. In Fig. 4(a) where $\epsilon/\omega = 0.5$, the second harmonic resonance occurs at $\Delta/\omega \approx 1.75$, and the third harmonic resonance occurs at $\Delta/\omega \approx 2.865$. As the bias increases to $\epsilon/\omega = 1.5$ in Fig. 4(b), the positions of the second and the third harmonic resonances shift to $\Delta/\omega \approx 1.25$ and $\Delta/\omega \approx 2.515$, respectively, which reflects the compensating effect between Δ and ϵ as demonstrated in Sec. III C. Moreover, as shown in Figs. 4(c) and 4(d), the second and the third harmonic resonances happen when $\tilde{\Omega}/\omega \approx 1$ and $\tilde{\Omega}/\omega \approx 2$, respectively, in agreement with the prediction of the CHRW method.

V. HIDDEN SYMMETRY

Now we come back to discuss the hidden symmetry of the asymmetric semiclassical Rabi model that appears as $\epsilon = m\omega, m \in \mathbb{Z}$. After careful calculation, we confirm that as $\epsilon = m\omega, m \in \mathbb{Z}$, the harmonic resonance of geometric quantities is absent for the numerical results at the third harmonic resonance Δ_{res}. Furthermore, we find that in this case, the geometric quantities are actually determined by the arbitrary choices of cyclic initial states. In this section we first illustrate this discovery using Floquet theory (about which we give a short overview in Appendix B 1). We also explain this
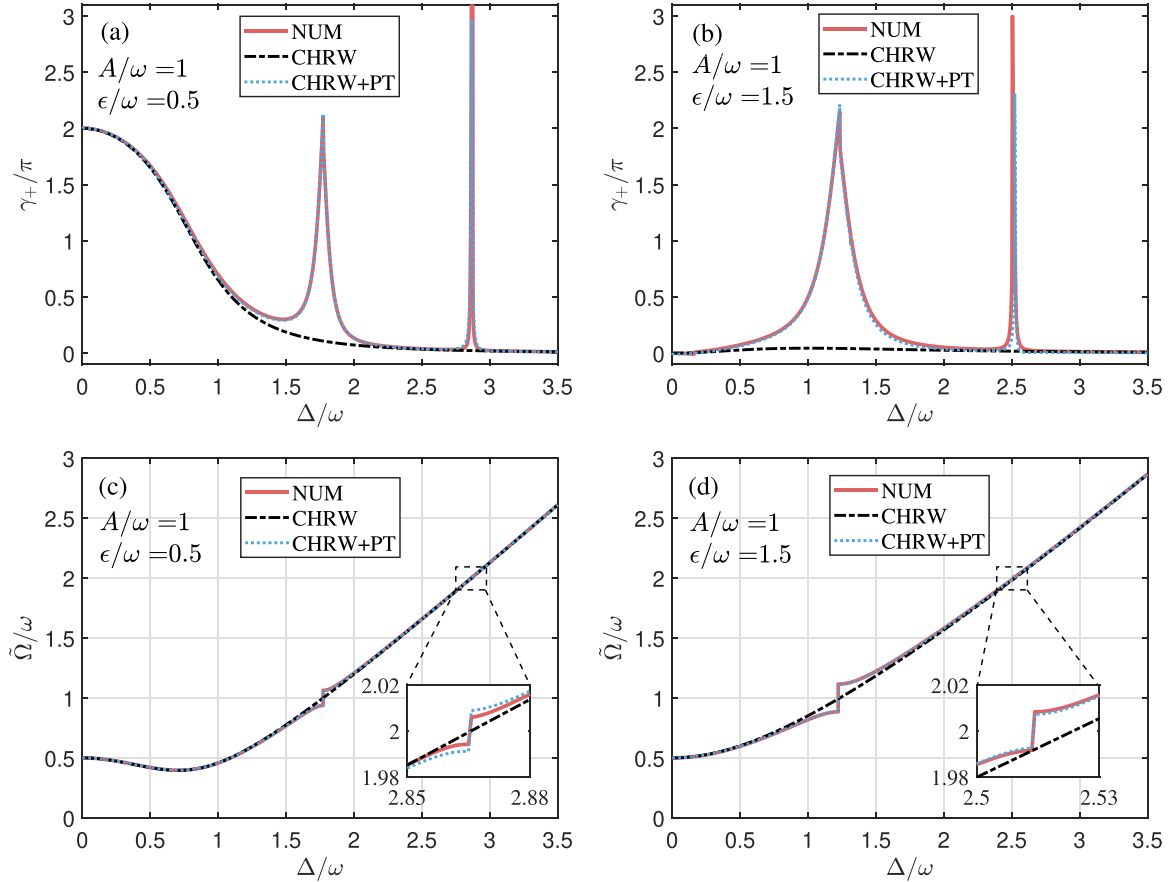
FIG. 4. (a), (b) AA phase γ_+/π as a function of Δ/ω for different values of ϵ/ω with $A/\omega = 1$ fixed: (a) $\epsilon/\omega = 0.5$; (b) $\epsilon/\omega = 1.5$. (c), (d) Modulated effective Rabi frequency $\tilde{\Omega}/\omega$ as a function of Δ/ω for different values of ϵ/ω with $A/\omega = 1$ fixed: (c) $\epsilon/\omega = 0.5$; (d) $\epsilon/\omega = 1.5$. The results of perturbation theory based on the CHRW method, denoted as CHRW+PT, agree well with the numerically exact results, while those obtained by CHRW show asymptotic tendency. In (c) and (d) we include magnified views to highlight the sudden changes at the harmonic resonance at $\tilde{\Omega}/\omega \approx 2$.

phenomenon in terms of hidden symmetry by comparing the asymmetric semiclassical Rabi model with the asymmetric quantum Rabi model.

First of all, one can numerically verify the fact that when $\epsilon = \omega$ and $\Delta = \Delta_{\text{res}}$, the quasienergies satisfy

$$q_- - q_+ = m\omega, m \in \mathbb{Z}, \qquad (62)$$

which is equivalent to

$$\theta_+ - \theta_- = 2m\pi, m \in \mathbb{Z}. \qquad (63)$$

According to Floquet theory, both quasienergies are physically identical, which means the quasienergies are degenerate, and any superposition of the cyclic initial states $|\Psi\rangle = c_1|\psi_-(0)\rangle + c_2|\psi_+(0)\rangle$ is also a cyclic initial state with the equivalent quasienergy [59], i.e.,

$$U(T)|\Psi\rangle = e^{-iq_+ T}|\Psi\rangle. \qquad (64)$$

Because $|\psi_-(0)\rangle$ and $|\psi_+(0)\rangle$ are linear independent, $|\Psi\rangle$ can be any state vector in the Hilbert space, and therefore the invariant space of $U(T)$ is the whole space. Thus we can naturally infer that $U(T) = e^{-iq_+ T}I$. Furthermore, combining Eq. (63) with the complementary relation $\theta_+ + \theta_- = 2l\pi, l \in \mathbb{Z}$, we can set $\theta_+ = \theta_- = 0$, without loss of generality, and in this case, $U(T) = I$.

Since the cyclic initial state can be, in principle, any vector in the Hilbert space, and geometric quantities which depend on it cannot be uniquely defined, we include AA phase and time-energy uncertainty as our focuses in this work. In this sense, the absent resonance obtained numerically is only one of the infinity solutions. It can be verified that the degeneracy of quasienergies as $\Delta = \Delta_{\text{res}}$ happens not only when $\epsilon = \omega$, but when $\epsilon = m\omega, m \in \mathbb{Z}$ as well.

This intriguing phenomenon stems from the hidden symmetry of the asymmetric Rabi model, which has been reported by a number of researchers for the asymmetric quantum Rabi model [54,64–66]. The Hamiltonian for the asymmetric quantum Rabi model can be written as

$$H_q = \omega a^\dagger a - \frac{g}{4}\sigma_z(a^\dagger + a) - \frac{\Delta}{2}\sigma_x - \frac{\epsilon}{2}\sigma_z, \qquad (65)$$

where ω is the frequency of a quantized resonator field with annihilation and creation operators a and $a^\dagger$, and g is the coupling strength between the qubit and the field. For this Hamiltonian, the hidden symmetry appears as long as $\epsilon = m\omega, m \in \mathbb{Z}$, and the conserved quantity which commutes with the Hamiltonian and corresponding symmetric unitary operator can be found in the case [64–66].

It is necessary to mention that the coefficients and signs chosen in Eq. (65) correspond to those in Eq. (1), and the properties of the asymmetric quantum Rabi model are not reliant on those particular choices. The quantum field in Eq. (65) can be reduced to the classical field in Eq. (1) with $g|\langle a\rangle| = A$ fixed and $g \to 0$, $|\langle a\rangle| \to \infty$, where $|\langle a\rangle|$ is expectation value of the annihilation operator a [67].

According to Floquet theory, the Floquet Hamiltonian for the asymmetric semiclassical Rabi model is

$$H_F = -\frac{\Delta}{2}\sigma_x - \frac{\epsilon + A\cos(\omega t)}{2}\sigma_z - i\partial_t. \qquad (66)$$

A comparison of Eqs. (66) and (65) in the matrix form demonstrates the similarity between the asymmetric semiclassical Rabi model and the asymmetric quantum Rabi model. For the asymmetric semiclassical Rabi model, we introduce a set of basis

$$|\uparrow\text{or}\downarrow, n\rangle = |\uparrow\text{or}\downarrow\rangle e^{-in\omega t}, \qquad (67)$$

where $|\uparrow\rangle$ and $|\downarrow\rangle$ are the eigenstates of σ_z. In the extended Hilbert space $\mathcal{H} \otimes \mathcal{T}$, those vectors become $|\uparrow\text{or}\downarrow, \mathrm{n}\rangle\rangle$ (see Appendix B 1 for the details). In this basis, the matrix of H_F reads

$$H_F = \begin{bmatrix}
\ddots & | \uparrow,-n\rangle\rangle & |\downarrow,-n\rangle\rangle & |\uparrow,-(n+1)\rangle\rangle & |\downarrow,-(n+1)\rangle\rangle & |\uparrow,-(n+2)\rangle\rangle & |\downarrow,-(n+2)\rangle\rangle \\
\hline
|\uparrow,-n\rangle\rangle & n\omega - \frac{\epsilon}{2} & -\frac{\Delta}{2} & -\frac{A}{4} & 0 & 0 & 0 \\
|\downarrow,-n\rangle\rangle & -\frac{\Delta}{2} & n\omega + \frac{\epsilon}{2} & 0 & \frac{A}{4} & 0 & 0 \\
|\uparrow,-(n+1)\rangle\rangle & -\frac{A}{4} & 0 & (n+1)\omega - \frac{\epsilon}{2} & -\frac{\Delta}{2} & -\frac{A}{4} & 0 \\
|\downarrow,-(n+1)\rangle\rangle & 0 & \frac{A}{4} & -\frac{\Delta}{2} & (n+1)\omega + \frac{\epsilon}{2} & 0 & \frac{A}{4} \\
|\uparrow,-(n+2)\rangle\rangle & 0 & 0 & -\frac{A}{4} & 0 & (n+2)\omega - \frac{\epsilon}{2} & -\frac{\Delta}{2} \\
|\downarrow,-(n+2)\rangle\rangle & 0 & 0 & 0 & \frac{A}{4} & -\frac{\Delta}{2} & (n+2)\omega + \frac{\epsilon}{2}
\end{bmatrix}. \qquad (68)$$

For the asymmetric quantum Rabi model, we introduce another similar set of basis,

$$|\uparrow\text{or}\downarrow, n\rangle, \qquad (69)$$

where $|\uparrow\rangle$ and $|\downarrow\rangle$ are the same as the symbols in Eq. (67), and $|n\rangle$ is the fork state for the periodic driving field. In this basis, H_q takes the form

$$H_q = \begin{bmatrix}
\ddots & |\uparrow,n\rangle & |\downarrow,n\rangle & |\uparrow,n+1\rangle & |\downarrow,n+1\rangle & |\uparrow,n+2\rangle & |\downarrow,n+2\rangle \\
\hline
|\uparrow,n\rangle & n\omega - \frac{\epsilon}{2} & -\frac{\Delta}{2} & -\frac{g}{4}\sqrt{n+1} & 0 & 0 & 0 \\
|\downarrow,n\rangle & -\frac{\Delta}{2} & n\omega + \frac{\epsilon}{2} & 0 & \frac{g}{4}\sqrt{n+1} & 0 & 0 \\
|\uparrow,n+1\rangle & -\frac{g}{4}\sqrt{n+1} & 0 & (n+1)\omega - \frac{\epsilon}{2} & -\frac{\Delta}{2} & -\frac{g}{4}\sqrt{n+2} & 0 \\
|\downarrow,n+1\rangle & 0 & \frac{g}{4}\sqrt{n+1} & -\frac{\Delta}{2} & (n+1)\omega + \frac{\epsilon}{2} & 0 & \frac{g}{4}\sqrt{n+2} \\
|\uparrow,n+2\rangle & 0 & 0 & -\frac{g}{4}\sqrt{n+2} & 0 & (n+2)\omega - \frac{\epsilon}{2} & -\frac{\Delta}{2} \\
|\downarrow,n+2\rangle & 0 & 0 & 0 & \frac{g}{4}\sqrt{n+2} & -\frac{\Delta}{2} & (n+2)\omega + \frac{\epsilon}{2}
\end{bmatrix}. \qquad (70)$$

The structural similarity between H_F and H_q is apparent in the matrix representation; note the exactly equal tridiagonal elements for both Hamiltonians [note that $n \in \mathbb{Z}^+$ for both matrices, and $-n$ is used in Eq. (68)]. Meanwhile, the off-tridiagonal elements of H_q depend on n and those of H_F depend on A, which is related to the average number of photons in the semiclassical limit [67,68]. However, in H_F, n runs from negative infinity to positive infinity, while in H_q, n cannot be negative because it labels the number of photons [39].

With the matrices of both Hamiltonians, we calculate the convergence values of the eigenvalues to obtain accurate energy spectra by incrementally increasing their dimensions. Figures 5(a) and 5(c) display the quasienergy of the asymmetric semiclassical Rabi model against Δ/ω, with $A/\omega = 1$ for $\epsilon/\omega = 1$ and $\epsilon/\omega = 0.8$, respectively, while Figs. 5(b)

and 5(d) show the eigenenergy of the asymmetric quantum Rabi model with $g/\omega = 1$, for $\epsilon/\omega = 1$ and $\epsilon/\omega = 0.8$. From these figures we can see that for $\epsilon/\omega = 1$, the quasienergies are degenerate at $\Delta_{\mathrm{res}}/\omega \approx 2.74$, and degeneracies can also be observed for the eigenenergy spectrum in the vicinity of $\Delta/\omega \approx 2.5$. However, no level crossing occurs when $\epsilon/\omega \neq 1$. Though not shown here, we also verified the general existence of level crossings for $\epsilon/\omega = m$, $m \in \mathbb{Z}$ and anticrossings for $\epsilon/\omega \neq m$, and we found that these characters were not influenced by the value of A/ω or g/ω, which mainly shifted the spectra along the Δ/ω axis. This fact provides strong evidence for the hidden symmetry of both the asymmetric semiclassical Rabi model and the asymmetric quantum Rabi model as structural properties of the Hamiltonian, which probably have impacts in all coupling regimes of light-matter interaction or driven two-level systems. Consequently, the hidden symmetry
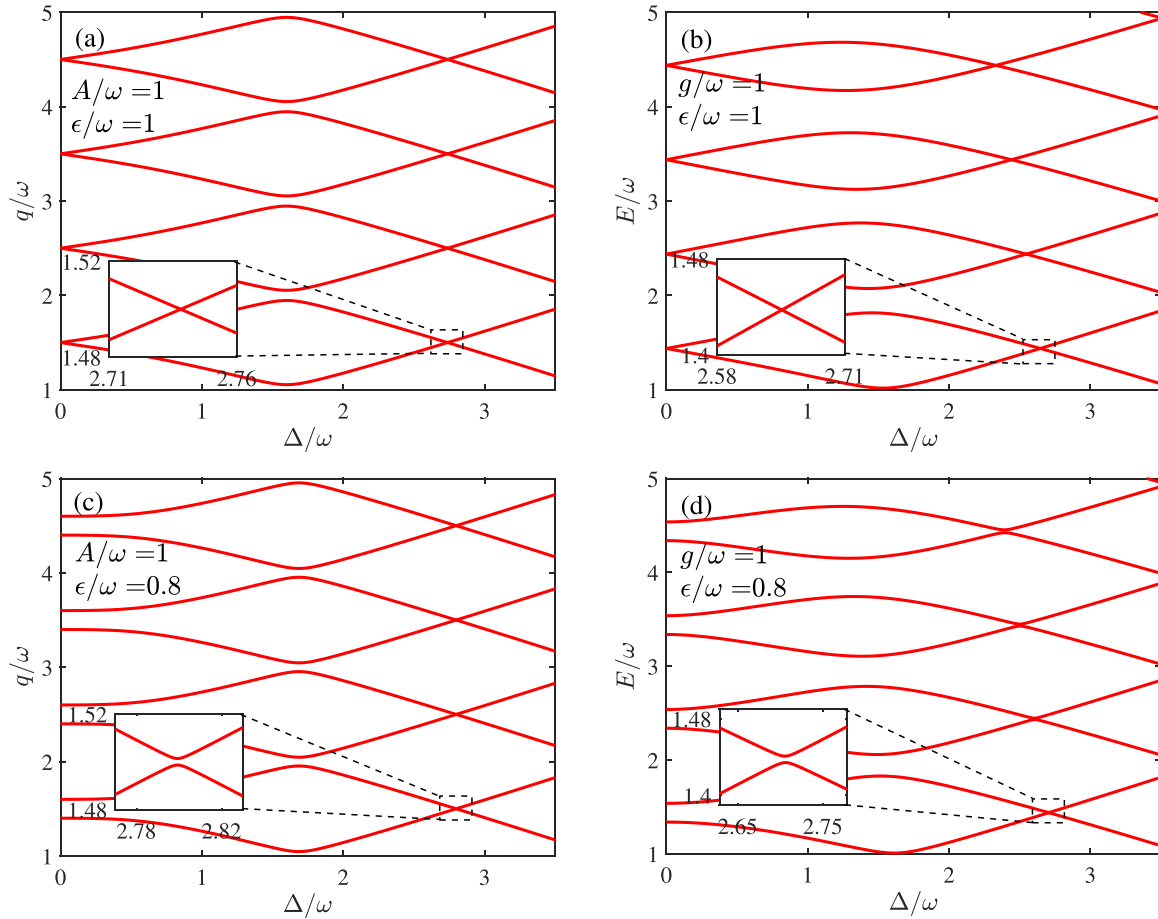
FIG. 5. Comparison of (quasi-)energy spectrum as a function of Δ/ω between the asymmetric semiclassical Rabi model and the asymmetric quantum Rabi model under different parameters. (a), (c) Quasienergy spectrum of the asymmetric semiclassical Rabi model with $A/\omega = 1, \epsilon/\omega = 1, 0.8$. (b), (d) Eigenenergy spectrum of the asymmetric quantum Rabi model with $g/\omega = 1, \epsilon/\omega = 1, 0.8$. For $\epsilon/\omega = 1$, the quasienergies or eigenenergies are degenerate at certain points, while no degeneracy occurs for $\epsilon/\omega = 0.8$.

contributes to the nonuniqueness of the geometric quantities, AA phase, and time-energy uncertainty.

VI. CONCLUSION

In this work we investigate the harmonic resonance of the AA phase and time-energy uncertainty as geometric quantities, and hidden symmetry in the asymmetric Rabi model by the numerical method. At the same time, we apply perturbation theory based on the CHRW method to analytically give an accurate time evolution operator and then calculate an accurate geometric phase, which is in good agreement with numerically exact results. The asymmetry in the Rabi model has important effects on the geometric phase. In comparison with the existence of only odd harmonic resonances in the absence of bias, various resonance phenomena take place in the presence of bias, including the emergence of the even higher-order harmonic resonances induced by the asymmetry, and the disappearance of odd higher-order resonance caused by the hidden symmetry present when $\epsilon = m\omega, m \in \mathbb{Z}$. Besides, with the increase of the bias, all the harmonic resonance shifts toward smaller values of Δ/ω owing to the compensating effect between ϵ and Δ, confirmed by both the

numerical method and the CHRW method using the condition $\tilde{\Omega} = m\omega, m \in \mathbb{Z}$.

We illustrate the features of harmonic resonance encapsulated by the repeated intersection of the AA phase at $\gamma = \pi$, attainment of a local maximum in time-energy uncertainty, and rapid oscillations in the population of the spin-up state, P_{up}. The harmonic resonance was mainly steered by the initial state $|\psi(0)\rangle$, which is highly sensitive to Δ/ω in the vicinity of harmonic resonance. The results obtained by the CHRW method, in which the influences of counter-rotating terms and bias were all taken into account in the rotating frame, exhibit asymptotic tendencies for both AA phase and modulated effective Rabi frequency. With the combination of perturbation theory, we further effectively depict the harmonic resonance peaks of γ_+ and sudden changes of $\tilde{\Omega}$ in the second and the third harmonic resonance regimes.

Upon investigation of the absence of harmonic resonance in the results of numerical calculation for $\epsilon = m\omega, m \in \mathbb{Z}, \Delta = \Delta_{res}$, we shed light on the dependence of geometric quantities on the choice of cyclic initial states due to the degeneracy of quasienergy of the asymmetric semiclassical Rabi model. Using Floquet theory, we found the structural similarity between H_F and H_q in the matrix representation and spectra, which reveals the hidden symmetry in the

asymmetric semiclassical Rabi model as an analogy of that in the asymmetric quantum Rabi model reported in Refs. [54,64–66]. Our results suggest that the hidden symmetry reflects the intrinsic property of the asymmetric Rabi model, regardless of the amplitude of the driving field or the coupling strength between the qubit and oscillating field, which plays a potential role in all coupling regimes of light-matter interaction or driven two-level systems. Meanwhile, since the time-energy uncertainty equals the length of path traversed by the state on the Bloch sphere, it can be measured in superconducting qubit systems via quantum process tomography.

ACKNOWLEDGMENT

APPENDIX A: PROJECTIVE HILBERT SPACE

In quantum mechanics, states are described by vectors in the Hilbert space $\mathcal{H}$. However, any two vectors $\psi, \phi \in \mathcal{H}$, satisfying

$$\psi = c\phi, c \in \mathbb{C}, \tag{A1}$$

are physically equivalent ($\psi \sim \phi$). Therefore the projective Hilbert space $\mathcal{P}$, defined as

$$\mathcal{P} := \mathcal{H}/\sim, \tag{A2}$$

is the proper space for representing quantum states that can be physically distinguished.

APPENDIX B: ANALYSIS OF HIDDEN SYMMETRY

1. Floquet theory

For a time-dependent Hamiltonian which satisfies $H(t + T) = H(t)$, the solution to the Schrödinger equation

$$i\partial_t |\psi(t)\rangle = H(t)|\psi(t)\rangle \tag{B1}$$

takes the form

$$|\psi_\alpha(t)\rangle = |u_\alpha(t)\rangle e^{-iq_\alpha t}, \tag{B2}$$

where q_α is called quasienergy, and $|u_\alpha(t + T)\rangle = |u_\alpha(t)\rangle$. This is often referred to as the Floquet theorem. Since $|\psi_\alpha(0)\rangle$ merely acquires a phase factor after $t = T$, i.e., the total phase $\theta = -q_\alpha T$, it is called a cyclic initial state. Inserting Eq. (B2) into Eq. (B1), the original problem can be transformed into an eigenvalue problem with Floquet Hamiltonian H_F:

$$H_F |u_\alpha(t)\rangle = [H(t) - i\partial_t]|u_\alpha(t)\rangle = q_\alpha |u_\alpha(t)\rangle. \tag{B3}$$

Note that the subscript α is to label the order of the eigenvectors or eigenvalues, but there are actually infinite set of solutions, because $|u_\alpha(t), n\rangle = e^{-in\omega t}|u_\alpha(t), 0\rangle \equiv e^{-in\omega t}|u_\alpha(t)\rangle$ is physically identical to Eq. (B2) only with the shifted quasienergy $q_{\alpha,n} \equiv q_\alpha - n\omega$. Thus, it is sufficient to consider the set of quasienergies within an interval of width ω and corresponding total phases within an interval of width 2π.

More importantly, H_F can be written as a time-independent infinite matrix through the expansion of the original Hilbert space $\mathcal{H}$ to $\mathcal{H} \otimes \mathcal{T}$ [39], where $\mathcal{T}$ contains all T-periodic

functions. A particular set of orthonormal complete basis in $\mathcal{T}$ is written as $\{|n\rangle\}$ with the plane-wave function

$$\langle t|n\rangle = e^{-in\omega t}. \tag{B4}$$

Considering a T-periodic state vector $|u_\alpha(t), n\rangle \in \mathcal{H}$, we can expand it in a Fourier series, plane-wave terms are derived

$$|u_\alpha(t), n\rangle = e^{-in\omega t}|u_\alpha(t)\rangle = \sum_l e^{-il\omega t}|u_\alpha^{(n-l)}\rangle, \tag{B5}$$

where $|u_\alpha^{(k)}\rangle$ are time-independent Fourier coefficients. Now in $\mathcal{H} \otimes \mathcal{T}$, the corresponding state vector is defined as

$$|u_\alpha, n\rangle\rangle \equiv \sum_l |u_\alpha^{(n-l)}\rangle \otimes |l\rangle, \tag{B6}$$

and finally the inner product is defined as

$$\langle\langle u_\alpha, n|u_\beta, m\rangle\rangle \equiv \frac{1}{T} \int_0^T dt \langle u_\alpha(t), n|u_\beta(t), m\rangle. \tag{B7}$$

2. Complementary relation of AA phases

To derive the complementary relation of AA phases, we start from the Schrödinger equation in Eq. (9). For this purpose, here we denote the Hamiltonian as $H(t) = [h_1, h_2; h_2, -h_1]$, where $h_1 = -(A\cos\omega t + \epsilon)/2$, $h_2 = -\Delta/2$, and $U(t) = [u_1, u_2; u_3, u_4]$. Then we can list the following ordinary differential equations (ODEs):

$$i\partial_t u_1 = h_1 u_1 + h_2 u_3, \tag{B8}$$

$$i\partial_t u_2 = h_1 u_2 + h_2 u_4, \tag{B9}$$

$$i\partial_t u_3 = h_2 u_1 - h_1 u_3, \tag{B10}$$

$$i\partial_t u_4 = h_2 u_2 - h_1 u_4, \tag{B11}$$

with boundary conditions:

$$u_1(0) = u_4(0) = 1,$$
$$u_2(0) = u_3(0) = 0.$$

Note that if we substitute the variables u_1 and u_2 in Eqs. (B10) and (B11) with u_4^* and $-u_3^*$, respectively, and take the conjugate of both equations, we will have the same equations as Eqs. (B8) and (B9), with the boundary conditions still satisfied. Due to the uniqueness theorem for ODEs, the relations

$$u_1 = u_4^*, \quad u_2 = -u_3^* \tag{B12}$$

must be kept in the solution for Eq. (9). Since the evolution operator is unitary, we can get

$$\begin{aligned}
U(t)U(t)^\dagger &= \begin{bmatrix} u_1 & u_2 \\ -u_2^* & u_1^* \end{bmatrix} \begin{bmatrix} u_1^* & -u_2 \\ u_2^* & u_1 \end{bmatrix} \\
&= \begin{bmatrix} |u_1|^2 + |u_2|^2 & 0 \\ 0 & |u_1|^2 + |u_2|^2 \end{bmatrix} \\
&= I, \tag{B13}
\end{aligned}$$

which implies that

$$det[U(t)] = |u_1|^2 + |u_2|^2 = 1, \forall t \geqslant 0. \tag{B14}$$

Because $e^{i\theta_+}$ and $e^{i\theta_-}$ are the two eigenvalues of $U(T)$, $e^{i\theta_+}e^{i\theta_-} = e^{i\theta_+ + \theta_-} = \det[U(T)] = 1$. Therefore we get the relation between total phases:

$$\theta_+ + \theta_- = 2l\pi, \, l \in \mathbb{Z}. \tag{B15}$$

Moreover, with Eqs. (B12) and (B14) it is easy to prove through some calculations that the two eigenvectors for $U(T)$, i.e., the cyclic initial states $|\psi_\pm(0)\rangle$, are orthogonal to each other, and thus

$$\langle\psi_-(0)|U^\dagger H U|\psi_-(0)\rangle = -\langle\psi_+(0)|U^\dagger H U|\psi_+(0)\rangle, \tag{B16}$$

which leads to

$$\alpha_- = -\alpha_+. \tag{B17}$$

Finally, we obtain from Eqs. (3), (4), (B15), and (B17) that $\gamma_+ + \gamma_- = 2l\pi, l \in \mathbb{Z}$.

APPENDIX C: PERTURBATION THEORY

Near the third harmonic resonance, $\tilde{\Omega} \approx 2\omega$. Thus the total phase given in Eq. (55) can be simplified as

$$\theta'_+ \approx \frac{\sqrt{1+k^2}(\tilde{\Omega}-2\omega)T - \omega T}{2}. \tag{C1}$$

By $\theta'_+ = \frac{\tilde{\Omega}'}{2}T + \frac{2n+1}{2}\omega T, n \in \mathbb{Z}$, we get the modified Rabi frequency

$$\tilde{\Omega}' \approx \sqrt{1+k^2}(\tilde{\Omega}-2\omega) + 2\omega. \tag{C2}$$

To calculate the dynamical phases, our target is to solve the integral in Eq. (30), since the total phases given by the CHRW method are reserved due to their tiny variation. In the first step we write the middle part of the integrand:

$$D^\dagger e^S H e^{-S} D = -\frac{\tau_y}{2}\left\{\frac{\sin\Theta}{x}[\nu(u\varepsilon - v\Delta) - \mu(u\Delta + v\varepsilon)]\right\} - \frac{\tau_x}{2}\left\{\cos^2\left(\frac{\Theta}{2}\right)(v^2\Delta - 2uv\varepsilon - u^2\Delta) + \frac{1}{x^2}\sin^2\left(\frac{\Theta}{2}\right)\right.$$

$$\left.\times[\Delta(\mu^2-v^2)-2\varepsilon\mu\nu]\right\} - \frac{\tau_z}{2}\left\{\cos^2\left(\frac{\Theta}{2}\right)(u^2\varepsilon - 2uv\Delta - v^2\varepsilon) + \frac{1}{x^2}\sin^2\left(\frac{\Theta}{2}\right)[\varepsilon(\mu^2-v^2)+2\Delta\mu\nu]\right\}. \tag{C3}$$

Next, we calculate the state vector at time t, using the evolution operator $\tilde{U}$ without perturbation:

$$\tilde{U}|\tilde{\psi}'_+(0)\rangle = \frac{1}{L}\begin{pmatrix} e^{-i\omega t/2}\left[(\tilde{A}+k\tilde{\delta})\cos\left(\frac{\tilde{\Omega}t}{2}\right) + i(\tilde{A}\sqrt{1+k^2}-k\tilde{\Omega})\sin\left(\frac{\tilde{\Omega}t}{2}\right)\right] \\ e^{i\omega t/2}\left[(k\tilde{A}-\tilde{\delta}-\sqrt{1+k^2}\tilde{\Omega})\cos\left(\frac{\tilde{\Omega}t}{2}\right) - i(\tilde{\Omega}+\sqrt{1+k^2}\tilde{\delta})\sin\left(\frac{\tilde{\Omega}t}{2}\right)\right] \end{pmatrix}, \tag{C4}$$

where the initial state under perturbation $|\tilde{+}'\rangle$ takes the form of Eq. (52) with all components $\tau_x, \tau_y,$ and τ_z taken into consideration.

To calculate the integral in Eq. (30) analytically, we also use ω to approximate $\tilde{\Omega}$, which leads to negligible effects. Last but not least, in the process, Taylor expansion is adopted:

$$\cos\left(\frac{\Theta}{2}\right) \approx 1 - \frac{1}{2}\left(\frac{\Theta}{2}\right)^2, \quad \sin\left(\frac{\Theta}{2}\right) \approx \frac{\Theta}{2}. \tag{C5}$$

Combining Eqs. (C3) and (C4) with the approximations above, we then calculate the dynamical phase given by perturbation theory:

$$\alpha'_+ \approx -\int_0^T \langle\tilde{\psi}'_+(0)|\tilde{U}^\dagger D^\dagger e^S H e^{-S} D\tilde{U}|\tilde{\psi}'_+(0)\rangle d\tau$$

$$\approx \frac{\pi}{2L^2}\left\{(\tilde{\delta}+\sqrt{k^2+1}\tilde{\Omega}-k\tilde{A})\left\{\frac{A^2\tilde{\delta}}{2\omega^3}[\epsilon(v^2-\mu^2)-2\Delta\mu\nu] - \frac{\tilde{\delta}}{128\omega}(3z^4-64z^2+512)(u^2\epsilon-2uv\Delta-v^2\epsilon)\right.\right.$$

$$\left. -\frac{2A\tilde{A}}{\omega^2}[(u\epsilon-v\Delta)v-(u\Delta+v\epsilon)\mu]+\frac{A\tilde{A}}{\omega}\left[\frac{2}{z}J_1(z)+1\right][k(u^2-v^2)+2uv]\right\}$$

$$\left. +\frac{4k}{x^2}J_2(z)(uv-v\mu)[k\tilde{A}(\tilde{\Omega}+\tilde{\delta})-(1+\sqrt{k^2+1})\tilde{\Omega}\tilde{\delta}-\sqrt{k^2+1}\tilde{\Omega}^2-\tilde{\delta}^2]\right\}. \tag{C6}$$

[1] M. V. Berry, Proc. R. Soc. London, Ser. A **392**, 45 (1984).

[2] P. J. Leek, J. M. Fink, A. Blais, R. Bianchetti, M. Goppl, J. M. Gambetta, D. I. Schuster, L. Frunzio, R. J. Schoelkopf, and A. Wallraff, Science **318**, 1889 (2007).

[3] D. J. Thouless, M. Kohmoto, M. P. Nightingale, and M. denNijs, Phys. Rev. Lett. **49**, 405 (1982).

[4] T. Oka and H. Aoki, Phys. Rev. B **79**, 081406(R) (2009).

[5] A. D. Cronin, J. Schmiedmayer, and D. E. Pritchard, Rev. Mod. Phys. **81**, 1051 (2009).

[6] Y. Aharonov and D. Bohm, Phys. Rev. **115**, 485 (1959).

[7] R. Resta, J. Phys.: Condens. Matter **12**, R107 (2000).

[8] X. Xie, M. Pu, J. Jin, M. Xu, Y. Guo, X. Li, P. Gao, X. Ma, and X. Luo, Phys. Rev. Lett. **126**, 183902 (2021).

[9] A. Leinonen, A. Hannonen, H. Partanen, J. Heikkinen, T. Setälä, A. T. Friberg, and T. K. Hakala, Commun. Phys. **6**, 132 (2023).

[10] X. X. Yi and J. L. Chang, Phys. Rev. A **70**, 012108 (2004).

[11] Z.-J. Ying, P. Gentile, J. P. Baltanás, D. Frustaglia, C. Ortix, and M. Cuoco, Phys. Rev. Res. **2**, 023167 (2020).

[12] C. A. Mead, Rev. Mod. Phys. **64**, 51 (1992).

[13] Y. Aharonov and J. Anandan, Phys. Rev. Lett. **58**, 1593 (1987).

[14] J. Anandan, Ann. Inst. Henri Poincare: Phys. Theorique **49**, 271 (1988).

[15] P. Z. Zhao, Z. J. Z. Dong, Z. X. Zhang, G. P. Guo, D. M. Tong, and Y. Yin, Sci. China Phys. Mech. Astron. **64**, 250362 (2021).

[16] X.-X. Yang, L.-L. Guo, H.-F. Zhang, L. Du, C. Zhang, H.-R. Tao, Y. Chen, P. Duan, Z.-L. Jia, W.-C. Kong, and G.-P. Guo, Phys. Rev. Appl. **19**, 044076 (2023).

[17] B.-J. Liu, L. L. Yan, Y. Zhang, M. H. Yung, S.-L. Su, and C. X. Shan, Phys. Rev. Res. **5**, 013059 (2023).

[18] J. Samuel and R. Bhandari, Phys. Rev. Lett. **60**, 2339 (1988).

[19] J. Anandan and Y. Aharonov, Phys. Rev. Lett. **65**, 1697 (1990).

[20] J. Anandan, Found. Phys. **21**, 1265 (1991).

[21] L. B. Levitin and T. Toffoli, Phys. Rev. Lett. **103**, 160502 (2009).

[22] F. Campaioli, F. A. Pollock, F. C. Binder, and K. Modi, Phys. Rev. Lett. **120**, 060409 (2018).

[23] A. del Campo, Phys. Rev. Lett. **126**, 180603 (2021).

[24] S. Sun, Y. Peng, X. Hu, and Y. Zheng, Phys. Rev. Lett. **127**, 100404 (2021).

[25] N. Margolus and L. B. Levitin, Physica D **120**, 188 (1998).

[26] S. Lloyd, Nature (London) **406**, 1047 (2000).

[27] A. C. Santos and M. S. Sarandy, Sci. Rep. **5**, 15775 (2015).

[28] S. P. Jordan, Phys. Rev. A **95**, 032305 (2017).

[29] S. L. Braunstein, Phys. Rev. Lett. **69**, 3598 (1992).

[30] V. Giovannetti, S. Lloyd, and L. Maccone, Phys. Rev. Lett. **96**, 010401 (2006).

[31] M. Zwierz, C. A. Pérez-Delgado, and P. Kok, Phys. Rev. Lett. **105**, 180402 (2010).

[32] V. Giovannetti, S. Lloyd, and L. Maccone, Nat. Photonics **5**, 222 (2011).

[33] I. Walmsley and E. Rabitz, Phys. Today **56**, 43 (2003).

[34] A. Carlini, A. Hosoya, T. Koike, and Y. Okudaira, Phys. Rev. Lett. **96**, 060503 (2006).

[35] S. Deffner and S. Campbell, J. Phys. A: Math. Theor. **50**, 453001 (2017).

[36] L. Garcia, J. M. Bofill, I. P. R. Moreira, and G. Albareda, Phys. Rev. Lett. **129**, 180402 (2022).

[37] I. I. Rabi, Phys. Rev. **49**, 324 (1936).

[38] I. I. Rabi, Phys. Rev. **51**, 652 (1937).

[39] J. H. Shirley, Phys. Rev. **138**, B979 (1965).

[40] P. W. Milonni, *An Introduction to Quantum Optics and Quantum Fluctuations* (Oxford University Press, Oxford, England, 2019).

[41] A. J. Leggett, S. Chakravarty, A. T. Dorsey, M. P. A. Fisher, A. Garg, and W. Zwerger, Rev. Mod. Phys. **59**, 1 (1987).

[42] Y. Dakhnovskii and R. Bavli, Phys. Rev. B **48**, 11020 (1993).

[43] Y. Dakhnovskii and H. Metiu, Phys. Rev. A **48**, 2342 (1993).

[44] M. S. Rudner, A. V. Shytov, L. S. Levitov, D. M. Berns, W. D. Oliver, S. O. Valenzuela, and T. P. Orlando, Phys. Rev. Lett. **101**, 190502 (2008).

[45] A. J. Ramsay, T. M. Godden, S. J. Boyle, E. M. Gauger, A. Nazir, B. W. Lovett, A. M. Fox, and M. S. Skolnick, Phys. Rev. Lett. **105**, 177402 (2010).

[46] C. F. Destefani, M. Villani, X. Cartoixà, M. Feiginov, and X. Oriols, Phys. Rev. B **106**, 205306 (2022).

[47] R. Manson, K. Roy-Choudhury, and S. Hughes, Phys. Rev. B **93**, 155423 (2016).

[48] D. Vion, A. Aassime, A. Cottet, P. Joyez, H. Pothier, C. Urbina, D. Esteve, and M. H. Devoret, Science **296**, 886 (2002).

[49] E. Il'ichev, N. Oukhanski, A. Izmalkov, T. Wagner, M. Grajcar, H. G. Meyer, A. Y. Smirnov, A. Maassen van den Brink, M. H. S. Amin, and A. M. Zagoskin, Phys. Rev. Lett. **91**, 097906 (2003).

[50] C. Deng, J.-L. Orgiazzi, F. Shen, S. Ashhab, and A. Lupascu, Phys. Rev. Lett. **115**, 133601 (2015).

[51] F. Grossmann, T. Dittrich, P. Jung, and P. Hänggi, Phys. Rev. Lett. **67**, 516 (1991).

[52] I. Goychuk and P. Hänggi, Adv. Phys. **54**, 525 (2005).

[53] Y. Chen, Z. Lü, Y. Yan, and H. Zheng, Phys. Rev. A **102**, 053703 (2020).

[54] D. Braak, Phys. Rev. Lett. **107**, 100401 (2011).

[55] F. Yoshihara, Y. Nakamura, F. Yan, S. Gustavsson, J. Bylander, W. D. Oliver, and J.-S. Tsai, Phys. Rev. B **89**, 020503(R) (2014).

[56] J. Hausinger and M. Grifoni, Phys. Rev. A **81**, 022117 (2010).

[57] Z. Lü, Y. Yan, H.-S. Goan, and H. Zheng, Phys. Rev. A **93**, 033803 (2016).

[58] S. Liu, Z. Lü, and H. Zheng, J. Phys. A: Math. Theor. **54**, 445302 (2021).

[59] A. N. Seleznyova, J. Phys. A: Math. Gen. **26**, 981 (1993).

[60] W. D. Oliver, Y. Yu, J. C. Lee, K. K. Berggren, L. S. Levitov, and T. P. Orlando, Science **310**, 1653 (2005).

[61] M. Grifoni and P. Hänggi, Phys. Rep. **304**, 229 (1998).

[62] T. Yabuzaki, S. Nakayama, Y. Murakami, and T. Ogawa, Phys. Rev. A **10**, 1955 (1974).

[63] N. Tsukada, T. Koyama, and T. Ogawa, Phys. Lett. A **44**, 501 (1973).

[64] V. V. Mangazeev, M. T. Batchelor, and V. V. Bazhanov, J. Phys. A: Math. Theor. **54**, 12LT01 (2021).

[65] C. Reyes-Bustos, D. Braak, and M. Wakayama, J. Phys. A: Math. Theor. **54**, 285202 (2021).

[66] Y.-F. Xie and Q.-H. Chen, J. Phys. A: Math. Theor. **55**, 225306 (2022).

[67] E. K. Irish and A. D. Armour, Phys. Rev. Lett. **129**, 183603 (2022).

[68] S. Ashhab, J. Phys. A: Math. Theor. **50**, 134002 (2017).